LABORATORY STUDY OF OIL SLICK SUBJECTED TO NEARSHORE CIRCULATION

By A. G. L. Borthwick[1] and S. A. Joynes[2]

ABSTRACT: This paper compares results from a simple numerical simulation of small-scale oil slick advection and spread (based on an equation of species coupled with wave-induced currents) with laboratory test data from a 3.5 × 6.0 m wave basin containing a sinusoidal beach profile. Dyed cedar wood oil provided clear visualizations of the experimental oil slick for analysis using a digital image processor. The numerical model predicted reasonably the nearshore circulation patterns and the movement of the oil slick. Even so, important discrepancies occurred, due to reflections from the experimental beach and the effect of surface tension–viscous spreading which were not included in the mathematical formulation. It should be noted that the small-scale results presented herein cannot be scaled up to prototype slicks that cover several surf zone widths.

INTRODUCTION

One of the worst forms of localized marine pollution results from an oil slick as it approaches a shoreline. Every stage in the marine ecosystem is severely affected. Studies by GESAMP ("Impact" 1977) and Kuiper et al. (1984) indicate that major reductions may occur in the numbers of aerobic organisms, phytoplankton, fish, and sea birds. Even the use of dispersants to weather the oil may be harmful to fish, as described by Swedmark et al. (1973).

Although municipal waste discharges exceed tanker spills by a factor of almost two (*Oil* 1985), oil spills from damaged oil tankers, oil pipelines, and offshore hydrocarbon installations have a dramatic and immediate environmental impact. With larger supertankers operating in congested sea lanes and increasing numbers of offshore structures reaching the end of their design lives, the risks of accidents have increased substantially in recent years. The Department of Energy (*Acops* 1991) has noted that 791 spills were reported off the coast of the United Kingdom in 1990 alone. Poignant examples of the dire consequences of such oil spills have been provided by the *Torrey Canyon*, *Amoco Cadiz*, and *Exxon Valdez* disasters in 1967, 1978, and 1989, respectively. In the case of the *Amoco Cadiz*, 223,000 metric tons of crude oil were spilled off the coast of Brittany. Strong onshore winds and an exceptionally high spring tide caused 320 km of the coastline to be contaminated. Three years later, significant oil pollution had effectively ceased offshore, but was still evident in sheltered estuaries and marshes, according to Gundlach et al. (1983).

Once a slick has occurred, it is immediately transported by wind, tide, current and wave processes while dispersing naturally. Later, its volume may be reduced by evaporation and droplet dispersion if surfactants are

[1]Lect., Dept. of Engrg. Sci., Univ. of Oxford, Parks Road, Oxford, OX1 3PJ, U.K.

[2]Sr. Engr., Barnett Consultants Ltd., Computational Hydr. Specialists, P. O. Box 9463, Hamilton, New Zealand.

Note. Discussion open until May 1, 1993. To extend the closing date one month, a written request must be filed with the ASCE Manager of Journals. The manuscript for this paper was submitted for review and possible publication on August 31, 1989. This paper is part of the ***Journal of Environmental Engineering***, Vol. 118, No. 6, November/December, 1992. ©ASCE, ISSN 0733-9372/92/0006-0905/$1.00 + $.15 per page. Paper No. 26999.

Downloaded from ascelibrary.org by National Tech University Of Athens on 10/26/19. Copyright ASCE. For personal use only; all rights reserved.

added to the slick. In contrast, water-in-oil emulsification may increase its effective volume. With time, the slick will spread unevenly, separate into a black surface layer trailed by a thin sheen, and perhaps break up into slicklets. In the wave breaker zone, tar balls form, due to a combination of vertical dispersion and sedimentation. The oil is finally broken down by oxidation, dissolution, and biodegradation. These processes have been described by various authors, e.g., Kolpack et al. (1977), Kuipers (1981), and Rasmussen (1985).

Advection, evaporation, and spreading processes dominate the initial behavior of the slick. Offshore, advection is primarily wind-driven. Nearshore, advection is also affected by wave-current interaction. In calm water, spreading is caused by imbalances in gravity-inertia, gravity-viscous, and surface tension–viscous forces (i.e., related to differences between the physical properties of the oil and water). Oil spread on the sea surface is also driven by flow characteristics, such as turbulence and current shears.

Huang (1983) and Spaulding (1988) have produced comprehensive reviews of oil spill modeling, which illustrate that wind-driven oil advection (being the primary advection process offshore) has been the subject of rather more research than wave-current advection. Winds are typically modeled by random walk, Markov chain, and meteorological simulations. Surface currents are usually obtained as the vectorial sum of wind-induced drift, tidal, residual, and wave-induced currents. Both Huang and Spaulding indicate that wave-current interaction in coastal regions leads to complex surface currents. Several techniques have evolved for oil spread modeling. One popular category is based on Fay's (1969) equations, which were originally derived from an order of magnitude analysis taking into consideration oil and water properties, and assuming calm water, constant oil volume, and isotropic motion. Fay's equations deal with the three spreading regimes and were later derived theoretically by Fannelop and Waldman (1971), using assumptions for viscous drag. Kuipers (1981) improved Fay's model by including oil viscosity and integrating forces over the dimensions of the slick. Rasmussen (1985) described an operational oil spill model for mass transport, heat transport, and physical and chemical processes. In the mass transport module, Rasmussen modeled spreading by means of Fay's equations, horizontal and vertical dispersion, evaporation, emulsification, and upwelling of dispersed oil droplets. Another category of oil spread model has evolved by drawing an analogy between turbulence and current shear-induced spreading and random Fickian diffusion. Strictly speaking, diffusion implies the interpenetration of oil and water as if oil were a dissolved constituent, whereas surface spreading involves growth in spill area directly related to its reduction in thickness. However, it may be reasonable to use the Fickian analogy with turbulent diffusion and convective dispersion (current shear). Flow-induced oil advection and spread processes may therefore be solved together using a conservation of species equation incorporating Fickian diffusion, as demonstrated by Murray (1972) and Kolpack et al. (1977). Both categories of oil spread model have their merits: Those based on Fay's equations are related directly to relative properties of oil and water, while Fickian models deal with the flow processes. However, the equation of species is capable of predicting the inhomogeneous shape of an oil slick in a current field and its local thickness, unlike Fay's equations. Kollmeyer and Thompson (1977) utilized the two-dimensional wind and tidal-induced current field to drive oil advection by means of a method of characteristics/finite difference solution of the species equation in an Eulerian frame of

Downloaded from ascelibrary.org by National Tech University Of Athens on 10/26/19. Copyright ASCE. For personal use only; all rights reserved.

reference. Hunter (1980) assumed spreading was caused only by turbulence and lateral velocity shears, and obtained favorable agreement with field data from a spill off Anglesey. He discretized the slick as a number of particles that were moved in a time-stepping Lagrangian scheme with spreading incorporated by means of random walks. Various authors, including Johansen (1985) and Elliott et al. (1986), have extended the Lagrangian methodology to move the oil as a distribution of buoyant droplets. Elliott et al. comment that it is physically unrealistic to model the initial oil spill as discrete droplets. Nevertheless, particle tracking approaches are straightforward to apply and give good agreement with observations when correctly tuned. Alternative Eulerian schemes based on spatial discretizations are able to simulate the continuous nature of a slick at early stages; they do require relatively fine mesh resolution, but this drawback is eroding with advances in computer technology.

A comprehensive coastal zone oil spill model has been developed by Reed et al. (1989) and tested by Reed and Gundlach (1989) against data from the *Amoco Cadiz* spill. Reed et al. divide the surface slick into discrete spillets which are advected by the vectorial sum of current components acting at the centroid, while spread by a modified formulation of Fay's gravity-viscous equation. Entrained subsurface oil is moved by discrete particle methods offshore and by use of a continuous Eulerian representation within the surf zone. Reed and Gundlach emphasize that resolution of the coastal morphology on its own is insufficient to improve model accuracy; local variations in longshore and rip currents must also be correctly simulated. Shen et al. (1987), Shen and Yapa (1988), and Yapa et al. (1989) describe relevant Lagrangian discrete parcel simulations of oil slick transport in rivers and lakes.

It is the purpose of this paper to present a simple combined wave-current interaction and conservation of species model for the wave-induced movement of a small-scale oil slick close to a beach with gradually varying profile. Wave reflection from the beach and diffraction are neglected. The governing mass and momentum equations are solved iteratively using an implicit finite difference procedure. Wave angles and wave heights are solved using explicit finite difference forms of the ray and energy equations, respectively. Once wave-current steady state is reached, the oil movement is simulated by solving the species equation using the method of characteristics for advection terms and central-differences for diffusion terms. Results from the numerical model are compared with experimental data from a spill in a laboratory wave basin containing a sinusoidal beach.

Governing Equations

Fig. 1 shows the Cartesian system adopted herein; η = the free-surface elevation above mean water level; $\bar{\eta}$ = the wave set-up or set-down; D = the mean water depth; θ = the wave angle; H = the wave height; and h = the still water depth. U and V = depth-averaged velocities in the x- and y-directions, respectively, where the x-direction is taken to be offshore from the beach, while the y-direction is longshore. For the wave-current model, it is assumed that the coastal waters under consideration are shallow relative to their horizontal dimensions. The wave field is described using linear wave theory in conjunction with the ray equation and a modified form of the conservation of energy equation to determine the wave angle and wave height, respectively. A full description of these equations has been given

Downloaded from ascelibrary.org by National Tech University Of Athens on 10/26/19. Copyright ASCE. For personal use only; all rights reserved.

Downloaded from ascelibrary.org by National Tech University Of Athens on 10/26/19. Copyright ASCE. For personal use only; all rights reserved.

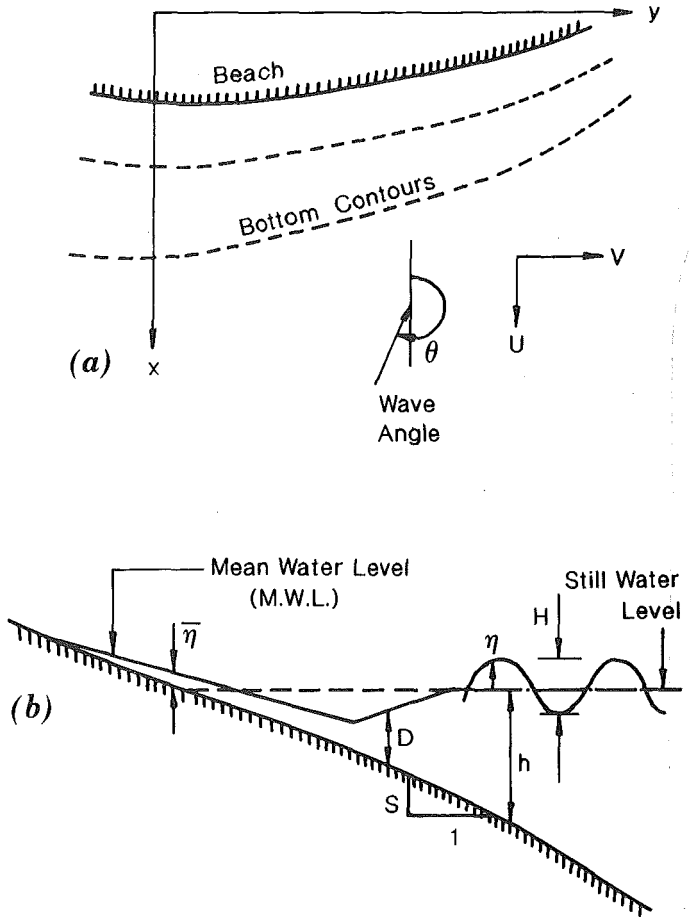

FIG. 1. Definition Sketches

by Borthwick and Joynes (1989). It should be noted that the breaking wave criterion used here is due to Battjes and Janssen (1978) and is given by

$$H_b = 0.14 \left(\frac{2\pi}{k_b}\right) \tanh\left(\frac{\gamma_b k_b h_b}{0.28\pi}\right) \quad \ldots\ldots\ldots\ldots\ldots\ldots\ldots\ldots\ldots\ldots (1)$$

where H_b = the breaking wave height; k_b = the wave number of the breaking wave; $\gamma_b = 0.8$; and h_b = the still water depth at breaking. Wave-current interaction is implemented using conservation of mass in conjunction with the Reynolds equations written in depth-averaged form. Although extremely important in field conditions, wind-induced surface stresses were not generated in the experimental tests; thus, the wind stress and Coriolis terms in the numerical scheme were not activated in this study. The bed shear stresses are estimated using a friction factor approach developed by Liu and Dalrymple (1978). The lateral (longshore) mixing coefficient ε_x, is obtained from a formulation related to the square of the wave height due

to Thornton (1970). The on/offshore mixing coefficient is approximated by a constant value.

Once the steady state wave-current regime is known, the surface velocity distribution is estimated from the depth-averaged currents using a simple formulation based on boundary layer theory. Using a 1/7th power law, the surface currents, u and v, are estimated as being 8/7 times the depth-averaged current velocities. It should be noted that the 1/7th power law is representative of open channel flow; Stive and Wind (1986) propose a more advanced formulation that accounts for boundary layer development in the surf zone. Moreover, Huang (1983) warned that depth-averaged currents may give a poor indication of surface currents, particularly if wind is present.

For comparison with the short-duration laboratory experiments, a simplified numerical model of the oil slick motion was developed that did not consider oil breakup, shearing between the oil and water surface, subsurface transport, oil viscosity, surface tension, temperature, emulsification, sedimentation, or evaporation. In the initial stages of the spill, this is reasonable (except for mechanical spreading caused by gravity-inertia, gravity-viscous, and surface tension–viscous forces, as we shall see later), and an advection-diffusion type equation (including the Fickian diffusion analogy) may be used to predict the movement of the oil slick. For an instantaneous surface oil thickness c, a two-dimensional conservation of species equation may be written (ignoring molecular diffusion) as

$$\frac{\partial c}{\partial t} + \frac{\partial (cu)}{\partial x} + \frac{\partial (cv)}{\partial y} = 0 \quad \ldots\ldots (2)$$

in which u and v = instantaneous surface velocities. The time-dependent quantities may be written as the sum of a mean quantity (overbar), a turbulent fluctuation (prime), and a wave-induced quantity (hat). Thus

$$u = \bar{u} + u' + \hat{u} \quad \ldots\ldots (3a)$$

$$v = \bar{v} + v' + \hat{v} \quad \ldots\ldots (3b)$$

$$c = \bar{c} + c' + \hat{c} \quad \ldots\ldots (3c)$$

These components are substituted into (2), which is then time-averaged, giving

$$\frac{\partial \bar{c}}{\partial t} + \bar{u}\frac{\partial \bar{c}}{\partial x} + \bar{v}\frac{\partial \bar{c}}{\partial y} = \frac{\partial}{\partial x}\left(E_x \frac{\partial \bar{c}}{\partial x}\right) + \frac{\partial}{\partial y}\left(E_y \frac{\partial \bar{c}}{\partial y}\right) \quad \ldots\ldots (4)$$

in which the total (diffusion-type) oil spread coefficients, E_x and E_y, are given by

$$E_x = K_x + W_x \quad \ldots\ldots (5a)$$

$$E_y = K_y + W_y \quad \ldots\ldots (5b)$$

K_x and K_y are (diffusion-type) coefficients of oil spread due to turbulence expressed by

$$\overline{u'c'} = -K_x \frac{\partial \bar{c}}{\partial x} \quad \ldots\ldots (6a)$$

$$\overline{v'c'} = -K_y \frac{\partial \bar{c}}{\partial y} \quad \ldots\ldots (6b)$$

Downloaded from ascelibrary.org by National Tech University Of Athens on 10/26/19. Copyright ASCE. For personal use only; all rights reserved.

and W_x and W_y are wave-induced (diffusion-type) coefficients of oil spread defined as

$$\overline{c'\hat{u}} + \overline{\hat{c}u'} + \overline{\hat{c}\hat{u}} = -W_x \frac{\partial \bar{c}}{\partial x} \quad \ldots\ldots\ldots\ldots\ldots\ldots\ldots\ldots\ldots\ldots (7a)$$

$$\overline{c'\hat{v}} + \overline{\hat{c}v'} + \overline{\hat{c}\hat{v}} = -W_y \frac{\partial \bar{c}}{\partial y} \quad \ldots\ldots\ldots\ldots\ldots\ldots\ldots\ldots\ldots\ldots (7b)$$

Eq. (4) represents transport of the oil slick by the two-dimensional velocity field. The right-hand side accounts for the influence of wave effects, as well as turbulence on the oil spreading process. The assumption that the mean correlated turbulent velocity and thickness fluctuations are proportional to mean thickness gradients is reasonable in (6). Eq. (7) also assumes that the mean correlated values of the wave-fluctuating and turbulent quantities are related to mean thickness gradients in a Fickian sense; this is included for simplicity in order to allow wave averaging, but is not physically justified. A more advanced numerical model (without wave-averaging) would, of course, do away with the need for (7).

Numerical Scheme

Fig. 2 shows the combination of coarse and fine meshes utilized by the overall numerical oil spill model. In Fig. 2, only a portion of the fine mesh is drawn; in fact, the mesh covered the entire flow field. The coarse grid is rectangular with spacings of $\Delta x = 0.2$ m; and $\Delta y = 0.35$ m and was used for the wave-current interaction computations. A detail of the grid is shown in Fig. 3. Here, $x = [i - (1/2)]\Delta x$; and $y = [j - 1(1/2)]\Delta y$. All variables are defined on the grid points, except U and V, which are centered on the midpoints of the x and y mesh lines. In order to improve the resolution of the oil spread, a refined square mesh with spacings of $\Delta x = \Delta y = 0.05$ m was nested within the coarse grid. Values of surface current required for the oil spread computations were transferred from the coarse to the refined mesh by linear interpolation.

In the first stage of the computational process, the numerical model simulated the refracted wave-current interactions until steady state resulted. This was achieved by means of an explicit finite difference solution of the wave angle and wave energy equations combined with an alternating direction implicit (ADI) solution of the depth-averaged continuity and nonlinear momentum equations. A full description of this part of the numerical model, including particulars of the boundary conditions, computational stability, etc., has been reported by Borthwick and Joynes (1989).

For the second part of the numerical scheme (when the oil was added to the steady state wave-current conditions), the species conservation equation was activated. The advection terms in (4) are hyperbolic, whereas the diffusion terms are parabolic. Thus, the solution of (4) in uncoupled form was obtained by a time-splitting procedure [see Holly and Usseglio-Polatera (1984)]. Considering the advection terms first, updated values were obtained initially in the x-direction, then in the y-direction by means of the method of characteristics. In this case, a fourth-order interpolation formula suggested by Crowley (1968) was implemented, giving, for the first computational sweep

$$\bar{c}^*_{i,j} = \bar{c}^n_{i,j} - \left\{\frac{\alpha}{12}\left[8(\bar{c}^n_{i+1,j} - \bar{c}^n_{i-1,j}) - (\bar{c}^n_{i+2,j} - \bar{c}^n_{i-2,j})\right]\right.$$

Downloaded from ascelibrary.org by National Tech University Of Athens on 10/26/19. Copyright ASCE. For personal use only; all rights reserved.

Downloaded from ascelibrary.org by National Tech University Of Athens on 10/26/19. Copyright ASCE. For personal use only; all rights reserved.

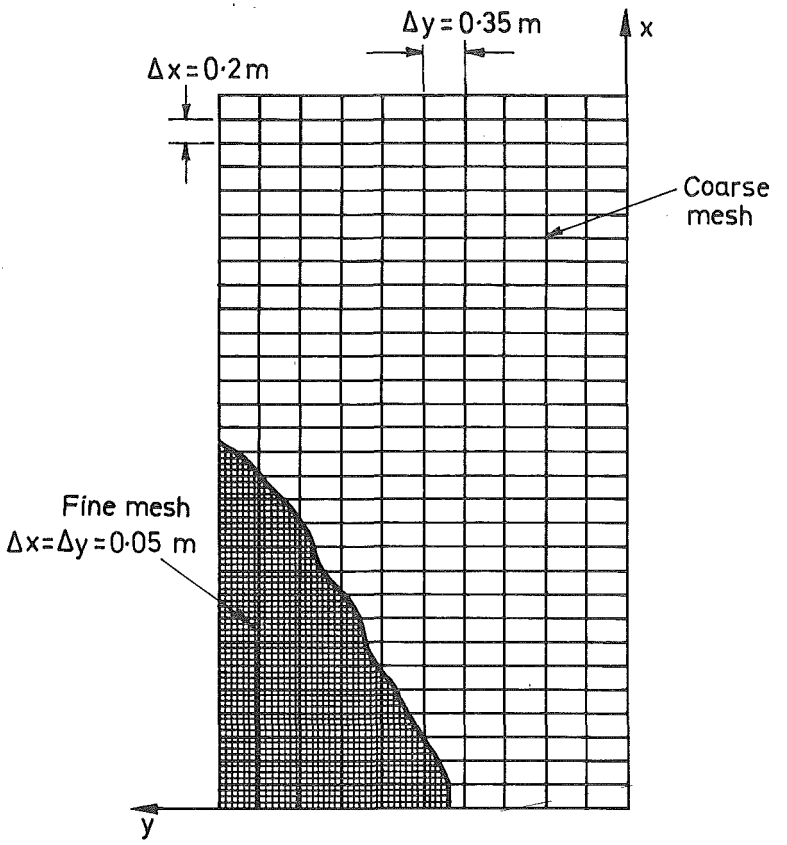

FIG. 2. Combined Meshes (Bounded by U and V Lines)

$$+ \frac{\alpha^2}{24}\left[30\bar{c}^n_{i,j} - 16(\bar{c}^n_{i+1,j} + \bar{c}^n_{i-1,j}) + (\bar{c}^n_{i+2,j} + \bar{c}^n_{i-2,j})\right]$$

$$+ \frac{\alpha^3}{12}\left[-2(\bar{c}^n_{i+1,j} - \bar{c}^n_{i-1,j}) + (\bar{c}^n_{i+2,j} - \bar{c}^n_{i-2,j})\right]$$

$$- \frac{\alpha^4}{24}\left[6\bar{c}^n_{i,j} - 4(\bar{c}^n_{i+1,j} + \bar{c}^n_{i-1,j}) + (\bar{c}^n_{i+2,j} + \bar{c}^n_{i-2,j})\right]\Bigg\} \quad \ldots\ldots\ldots\ldots\ldots (8)$$

then, for the second computational sweep

$$\bar{c}^{\dagger}_{i,j} = \bar{c}^*_{i,j} - \Bigg\{\frac{\alpha_1}{12}\left[8(\bar{c}^*_{i,j+1} - \bar{c}^*_{i,j-1}) - (\bar{c}^*_{i,j+2} - \bar{c}^*_{i,j-2})\right]$$

$$+ \frac{\alpha_1^2}{24}\left[30\bar{c}^*_{i,j} - 16(\bar{c}^*_{i,j+1} + \bar{c}^*_{i,j-1}) + (\bar{c}^*_{i,j+2} + \bar{c}^*_{i,j-2})\right]$$

$$+ \frac{\alpha_1^3}{12}\left[-2(\bar{c}^*_{i,j+1} - \bar{c}^*_{i,j-1}) + (\bar{c}^*_{i,j+2} - \bar{c}^*_{i,j-2})\right]$$

Downloaded from ascelibrary.org by National Tech University Of Athens on 10/26/19. Copyright ASCE. For personal use only; all rights reserved.

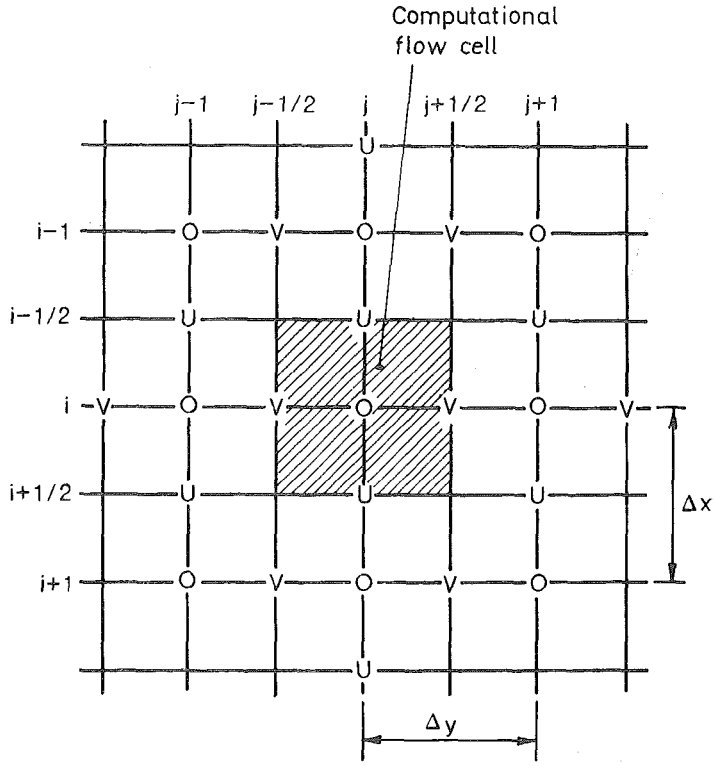

FIG. 3. Detail of Grid System

$$- \frac{\alpha_1^4}{24} [6\bar{c}^*_{i,j} - 4(\bar{c}^*_{i,j+1} + \bar{c}^*_{i,j-1}) + (\bar{c}^*_{i,j+2} + \bar{c}^*_{i,j-2})]\Big\} \quad \ldots\ldots\ldots\ldots (9)$$

where time $t = n\Delta t$; n = the time increment number; Δt = the time step; $\alpha = u_{i,j}\Delta t/\Delta x$; $\alpha_1 = v_{i,j}\Delta t/\Delta y$; and superscripts * and † = values calculated after the x and y sweeps between time increments n and $n + 1$.

The spreading terms were then approximated by central differences in space and forward differences in time, giving, for the final sweep

$$\bar{c}^{n+1}_{i,j} = \bar{c}^{\dagger}_{i,j} + \Delta t \left[\frac{K_x(\bar{c}^{\dagger}_{i+1,j} - 2\bar{c}^{\dagger}_{i,j} + \bar{c}^{\dagger}_{i-1,j})}{\Delta x^2} + \frac{K_y(\bar{c}^{\dagger}_{i,j+1} - 2\bar{c}^{\dagger}_{i,j} + \bar{c}^{\dagger}_{i,j-1})}{\Delta y^2} \right]$$

$$\ldots\ldots\ldots\ldots (10)$$

To maintain stability for the advection steps, α and α_1 must be less than unity. In this case, Δt was constrained by setting $\Delta t = 0.95\Delta x/|\text{Vel}_{\max}|$ where $|\text{Vel}_{\max}|$ = the magnitude of the highest velocity in the current field.

Experimental Arrangement

To examine the behavior of an oil slick under controlled conditions, an experimental wave basin was constructed in the Hydraulics Laboratory of

the Department of Civil Engineering at the University of Salford, England. The tank has an overall plan area of 3.50 m × 7.24 m and is supported 0.7 m above the laboratory floor by seven blockwork walls. The base of the tank consisted of two thicknesses of plywood supported on timber beams. Sheets of Perspex, 18 mm thick, formed the side walls. These were reinforced by steel angles augmented by a tensioned screw mechanism to prevent distortion of the walls by hydrostatic pressure for water depths up to 0.4 m.

Regular waves were produced at one end of the basin by a piston-type paddle driven by a 4 hp, 500 rpm variable-speed motor, coupled with a 4:1 reduction gear via a toothed belt and pulley system. A circular cam wheel mounted on the main drive shaft provided the periodic motion of the paddle. The paddle moved on steel tracks supported independently from the wave tank in order to reduce vibration effects from the motor. At the other end of the basin, the wave energy was dissipated on an upper plane Hairlok beach of 0.375 slope. This meant that the maximum plan area of the water surface was restricted to 3.5 × 5.0 m between the plane spending beach and paddle generator.

A half periodic sinusoidal lower beach was fabricated, ensuring that circulation patterns developed in accordance with the findings of Noda (1974) and da Silva Lima (1981). The equation used to design the lower beach, shown in Fig. 4, is given by

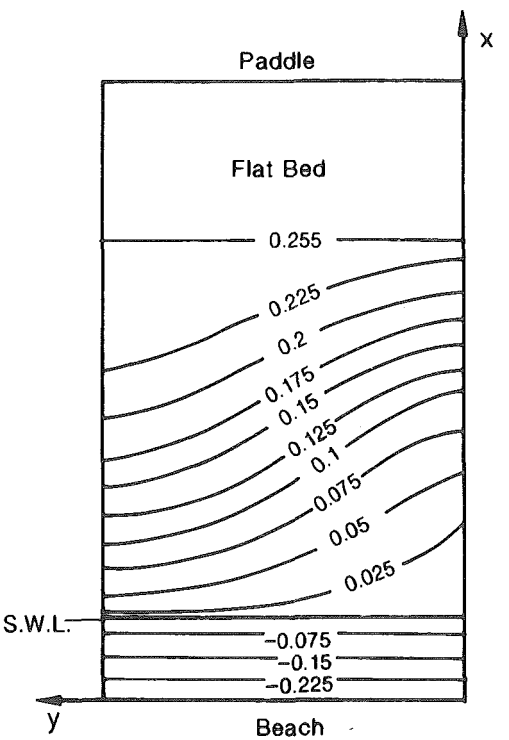

FIG. 4. Model Bathymetry

Downloaded from ascelibrary.org by National Tech University Of Athens on 10/26/19. Copyright ASCE. For personal use only; all rights reserved.

$$h(x, y) = s\left[x - 0.875 \sin\left(\frac{\pi x}{3.5}\right) \sin\left(\frac{2\pi y}{\lambda}\right)\right] \quad \ldots\ldots\ldots\ldots\ldots\ldots (11)$$

where the beach gradient $s = 0.0714$; and the rip current spacing $\lambda = 7$ m. The sinusoidal beach had a timber base and was covered with aluminium plates to provide a sturdy, warp-free surface. After fabrication, the lower sinusoidal beach and flat bed were painted light blue to contrast with the dyed oil. For the experimental study described in this paper, the deep water depth was 0.255 m at the paddle. A wire grid with 0.2 m and 0.35 m spacings in the offshore x-direction and longshore y-direction, respectively, corresponding to the numerical mesh, was located over the wave basin.

Before any waves were generated, the still water depth was measured at each grid node using an Armfield depth gage accurate to 1 mm. This allowed the input bathymetry data for the numerical model to be corrected for small differences between the designed and as-constructed depth contours. Here, the still water line was taken to be at the intersection between the plane spending beach and the periodic beach.

All data involving the wave-current characteristics and oil spreading were collected at least 20 min after the wave generator was switched on. This enabled the wave-current field to reach adequate steady-state conditions. The wave period was obtained by timing the passage of 10 waves in the vicinity of the paddle. At each grid node, the wave height was measured using a capacitance wave gage connected to an oscilloscope and amplifier. Surface currents were determined from a freeze-frame analysis of video film taken by an overhead camera of the trajectories of floats added to the basin. The floats consisted of weighted circular wooden discs with a density equal to 930 kg/m^3; their performance had previously been checked (Joynes 1989) against known velocities. The camera was located 5.7 m above the wire mesh (5.9 m above the still water depth). This gives rise to a maximum angular parallax error of just under 3% for the farthest grid point.

After a sensitivity study involving a number of different oils and dyes, it was found that a combination of 25 ml of cedar wood oil dyed with 0.7 g of Sudan Black dye was most adequate for modeling purposes. Cedar wood oil has a density of 950 kg/m^3 and was observed to spread mechanically at a suitable rate in still water, bearing in mind the relatively small dimensions of the wave basin. Uniformity of color was also achieved for a given oil thickness. An evaporation loss test indicated that negligible mass loss occurred over the duration of the main spill test. A still water oil diffusion coefficient (based on the assumption that spreading could be modeled as a Fickian diffusion process) was determined from a test in which oil was spilled in water that had not been disturbed for at least 12 hr.

During the main test, once steady-state wave-current conditions had been reached, the dyed oil was spilled from a beaker into the basin at an elevation of no more than 4 cm above the water surface. The spill was classified as instantaneous since it was added in less than one second. Its location was 3.7 m offshore from the still water line, and $y = 1.4$ m alongshore near the beginning of the onshore rip current. This was selected by trial and error so that oil did not spread to the side walls during the early stages of the test.

The overhead video camera then recorded the dispersion of the spill until the oil was no longer visible. This took approximately 5 min to occur. In order to minimize light reflections, all natural light was blacked out and two 2 kW photographic lamps were installed. After each oil spill test, the wave

Downloaded from ascelibrary.org by National Tech University Of Athens on 10/26/19. Copyright ASCE. For personal use only; all rights reserved.

basin was completely emptied, cleaned, and refilled with fresh water to avoid any subsequent surface tension effects from oil residue.

The video data were enhanced and freeze-frame analyzed by means of a digital image processor. In essence, frames of interest (selected at intervals of one wave period) were digitized using a minicomputer. The image produced related to a plan area measuring 4 m × 4 m, and consisted of 512 × 512 pixels. A pixel therefore corresponded to a resolution of 0.008 m × 0.008 m. Each pixel was given a two-dimensional address for scaling and location purposes. Electromagnetic energy generated from the original image was used to give each pixel an integer-intensity value ranging from 0 to 256 (with 0 corresponding to the darkest). To obtain consistent results, the image was contrast-stretched over the three color bands; namely, red, green, and blue. For example, red integer intensity values were stretched from 35–190 to 0–256.

A density slicing procedure was then applied to each image so that the oil thickness contours could be calibrated using information from earlier still water tests. Pixel value ranges (and thus oil thickness contours) were then colored to obtain a sharp image. For example, pixel values from 1–10, 10–40, and 40–80 referred to oil thicknesses of >64 μm, 12–64 μm, and 6–12 μm, and were coded red, white, and blue, respectively. A color copy was then printed, and oil thickness contour lines drawn. Thus, a picture of the wave-averaged spread of the slick was obtained.

Results

Nearshore Circulation

Regular waves were generated with period 1.29 s and offshore deep water wave height of 0.098 m (at the paddle) in both the numerical and physical models. A time step of 0.255 s was selected for the numerical computations, corresponding to a Courant number equal to unity. In order to prevent numerical seiching, the deep water wave height was built up over 3.823 s (related to the first harmonic resonant sloshing frequency in the basin). The lateral mixing coefficient ε_y had a value of 0.0376 m²/s. The bed stress was obtained using an estimated friction factor equal to 0.037.

Simulated and observed steady state nearshore circulation patterns are shown in Fig. 5. The experimental data refer to surface currents, whereas the numerical data are depth-mean values. It should therefore be noted that the surface values are approximately 15% larger than depth-averaged values, and this is taken into account in the following discussion. Overall, the clockwise rotating primary circulation patterns are in close agreement, with an offshore current occurring between $y = 2.3$ m and $y = 3.0$ m alongshore. The center of circulation in the experimental basin is somewhere between 2.4 and 3.4 m offshore, at $y = 2$ m across the basin. This compares with the numerical prediction, which is 2.8 m offshore from the still water line and at $y = 2.4$ m.

Although the experimental results indicate a strong counterclockwise secondary circulation within the surf zone at $x = 1.65$ m and $y = 2.5$ m, the numerical model underestimates the magnitude of currents close to the beach, which reduces the secondary circulation cell. However, the predicted rip currents at the sides of the primary cell are larger than found experimentally. These effects are due mainly to wave reflections, which were not simulated in the numerical model; it is recommended that the simple wave ray formulation used herein be replaced by a more comprehensive approach, such as proposed by Copeland (1985) based on the mild slope equation,

Downloaded from ascelibrary.org by National Tech University Of Athens on 10/26/19. Copyright ASCE. For personal use only; all rights reserved.

Downloaded from ascelibrary.org by National Tech University Of Athens on 10/26/19. Copyright ASCE. For personal use only; all rights reserved.

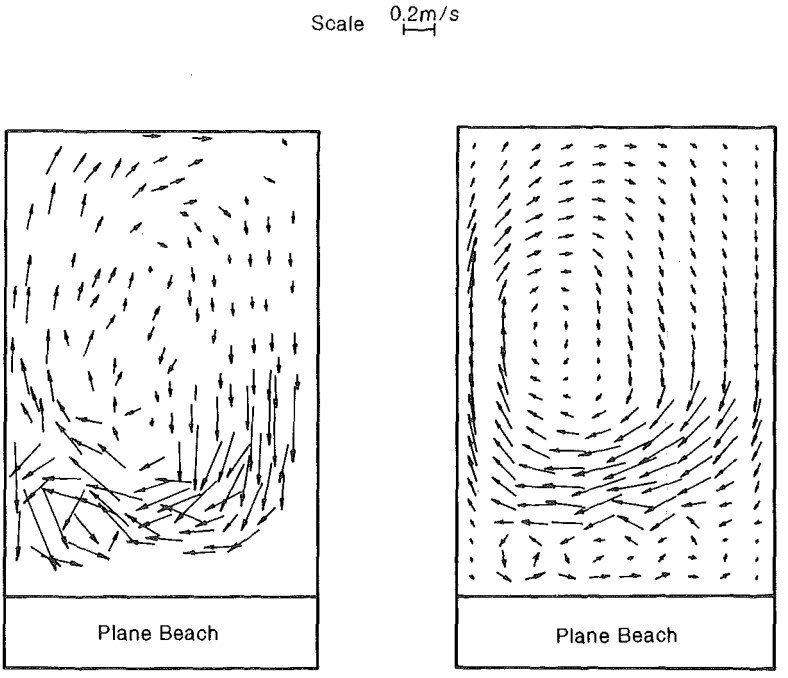

FIG. 5. Circulation Patterns: (*a*) Experimental; (*b*) Numerical

which models wave reflection and diffraction as well as refraction. Moreover, the ADI scheme itself creates a smoother representation of the circulation patterns and does not correctly simulate sharp turns of current. This smoothing is caused by the implicit scheme eliminating energy transfer processes governed by the nonlinear terms in the momentum equations. As Borthwick and Joynes (1989) have shown, an explicit scheme would have modeled better the jetting effects exhibited in the experimental data, but at the cost of computational instability.

Fig. 6 shows the measured and predicted steady state wave heights as a function of distance offshore away from the still water line along $y = 1.225$ m. In general, there is reasonable correlation between the test data and numerical predictions, although the numerical simulation has again smoothed out some of the observed behavior. In the nearshore zone, the wave heights are consistently underpredicted at the position of maximum longshore current. This is due mainly to reflections from the test beach, which caused an antinode of a standing wave to form in the surf zone. Other experimental factors, which contributed to the discrepancies between the measured and predicted data, include the influence of paddle vibrations (particularly at multiples of the wave frequency) and edge waves (derived from reflected and standing wave components from the nonporous beach, paddle, and side walls).

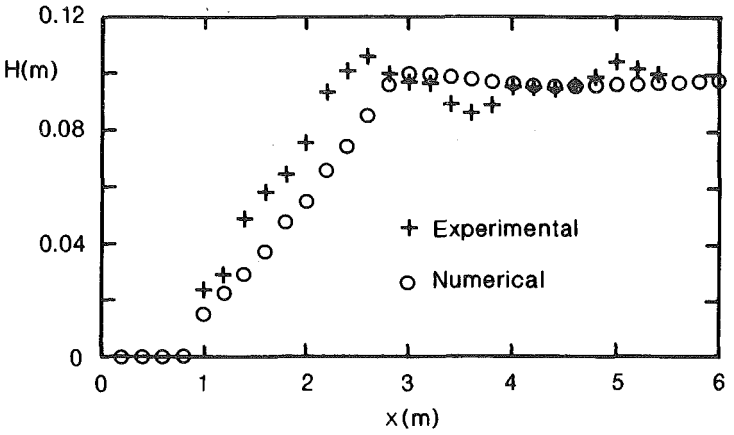

FIG. 6. Offshore Wave Height Distribution at y = 1.225 m

Oil Slick Behavior

The initial experimental slick covered an area of 0.1475 m^2 (59 grid points in the refined mesh). Input oil thickness values for the numerical model were obtained by interpolation from the experimental data using the digital image processor. The inner slick was assumed to have an exponential distribution of thickness dependent on the still water oil diffusion coefficient. In order to compensate for the positional differences between the experimental and numerical circulation cells, the initial numerical spill was located 3.0 m offshore from the still water line at y = 1.7 m; the foregoing values were calculated by multiplying the experimental distances by the ratio of the theoretical to experimental distances to the center of the circulation cells (taking the experimental offshore value to be 3.4 m in this case). Fig. 7 shows the wave-averaged movement of the experimental and numerical slicks over 38.7 s (30 wave periods) from the initial spill. Allowing for the disparity between the centers of the nearshore circulation cells, it may be judged that the two advection paths are in reasonable agreement.

Turning to the oil spreading processes, a sensitivity study (assuming isotropy) indicated that the total oil diffusion coefficient, $E = E_x = E_y$, had a value equal to 0.0004 m^2/s. It is worth noting that comparisons with field data by Murray (1972) and Hunter (1980) indicated E values of 15 m^2/s and 5 m^2/s, respectively. The large differences between the field and experimental coefficients underline the importance of scale effects, e.g., oil density, surface tension, turbulent eddy sizes, etc., discussed later. Fig. 7 shows that up to a time of 11.61 s (9 wave periods) from the initial spill, the predicted and experimental slicks were similar in shape as they approached the shoreline, being advected by the onshore current. The longshore current played a considerable role in spreading the oil close to the breaker line for times between 15.48 and 23.22 s (12 and 18 wave periods). At 12 wave periods, the physical slick became more or less circular. Then, as the slick was advected further alongshore, the rip current began to stretch the slick in the y-direction, resulting, at 18 wave periods, in an elliptical shape with the major axis double the length of the minor axis. In contrast, the simulated slick was stretched in the y-direction by the longshore current until it reached the entrance of the rip current at 18 wave periods. Differences in the physical and numerical slick shapes may be explained partly by the discrepancies in

Downloaded from ascelibrary.org by National Tech University Of Athens on 10/26/19. Copyright ASCE. For personal use only; all rights reserved.

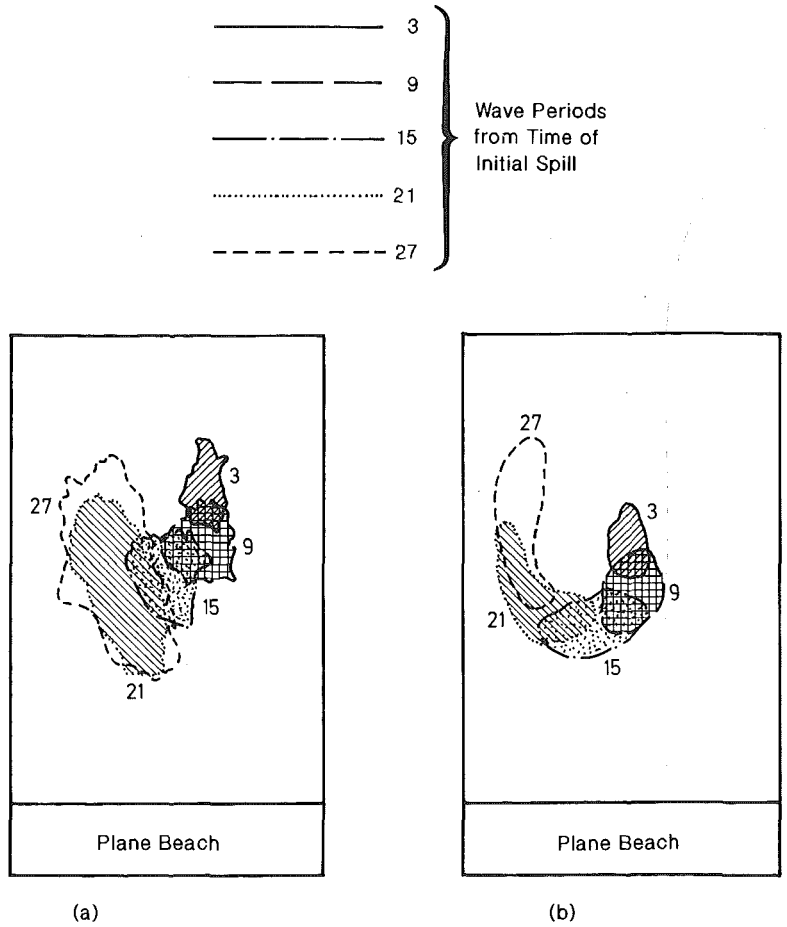

FIG. 7. Temporal Development of 6 μm Oil Thickness Contours: (*a*) Experimental; (*b*) Numerical

modeling wave-current interaction (discussed previously), and by the assumption that an analogy with Fickian diffusion could explain spreading by current shears and turbulence, while ignoring mechanical spreading due to the relative physical properties of oil and water. In particular, the numerical model did not represent surface tension–viscous spreading, which is important for small-volume experimental oil spills. Furthermore, the coarse grid numerical model was unable to simulate the breakup of the slick at the edge of the surf zone. The experimental oil slick remained behind the breaker line, but was still advected by the longshore current due to the overall circulation pattern. Since the influence of the longshore current was relatively small outside the surf zone, the slick was not stretched appreciably in the lateral direction. As soon as the oil entered the rip current, which was flowing through the breaker line, it was immediately spread offshore. On the other hand, the simulated slick entered the surf zone where the relatively stronger longshore current spread the oil alongshore.

Downloaded from ascelibrary.org by National Tech University Of Athens on 10/26/19. Copyright ASCE. For personal use only; all rights reserved.

From both sets of data, it may be observed that on entering the rip current, the slick elongated offshore towards the paddle. This situation occurred between 27.09 and 34.83 s (21 and 27 wave periods). It is evident that the numerical model predicts reasonably the offshore length of the slick (approximately 2.2 m) implying that the rip current moved the oil at approximately the same rate in the x-direction. It should be noted, nevertheless, that the numerical model underestimated the lateral spread of the slick.

Fig. 8 shows the temporal growth in area of that portion of the oil slick of thickness greater than or equal to 6 μm. It is clear that the areal dimensions of the physical slick increase more rapidly than predicted by the numerical model. Several factors are responsible for this, the most important being the insensitivity of the species formulation, as used herein, to the relative physical properties of the oil and water. For the small volume of oil considered here, Fay's (1969) equations indicate that surface tension–viscous spreading phase occurs almost immediately after the spill is initiated. A plot of the overall slick area calculated using Fay's equations, shown in Fig. 9, underlines the importance of mechanical spreading. Future studies should seek to find a way of linking mechanical spreading [perhaps, in the general form proposed by DiPietro et al. (1978)] to the flow dynamics by means of a modified conservation of species equation. Another factor that may enhance the spreading rate is the mixing effect of small eddies generated in the shear layers at the sides of the rip current. The spatial variation in turbulence intensity would be better modeled by a depth-averaged two-(k-ε) turbulence model.

Scale Effects

Sea waves are relatively straightforward to model, being gravity-dependent and thus obeying Froude's law of scaling. For typical granular beaches, wave energy is absorbed and so wave reflections would be very much less than obtained from small-scale experiments with impermeable beaches. This means that the hydrodynamic simulation of nearshore circulation should be appropriate for prototype applications. Moreover, the results from the laboratory wave basin are suitable for validation of the numerical model.

Turning to the oil spill, at its earliest stages, spreading is dominated by the relative magnitudes of gravity, inertia, viscous, and surface-tension forces.

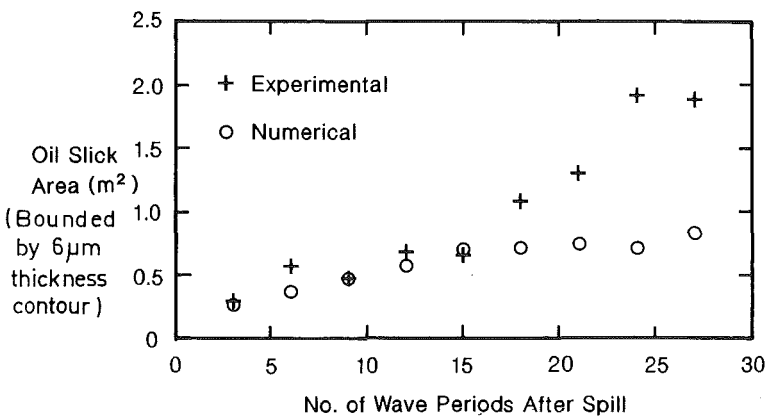

FIG. 8. Growth of Oil Slick Area (>6 μm Thickness)

Downloaded from ascelibrary.org by National Tech University Of Athens on 10/26/19. Copyright ASCE. For personal use only; all rights reserved.

Downloaded from ascelibrary.org by National Tech University Of Athens on 10/26/19. Copyright ASCE. For personal use only; all rights reserved.

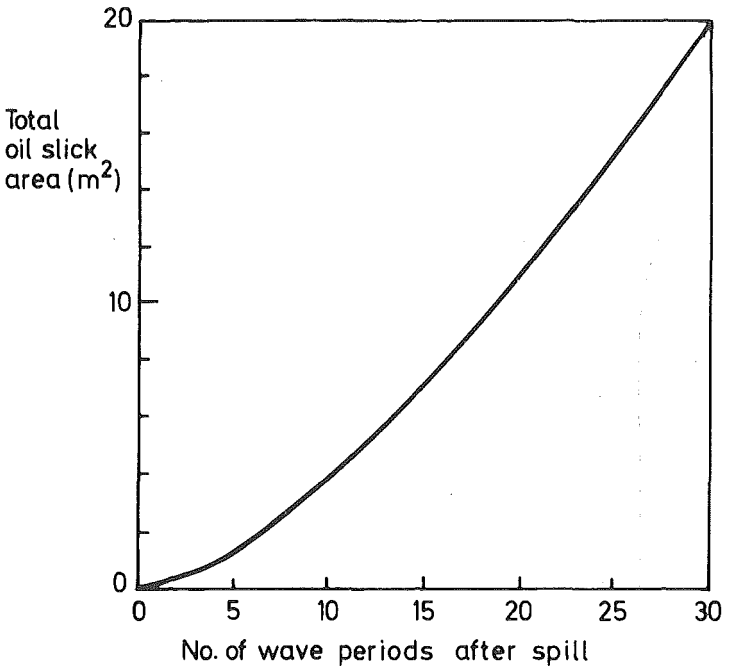

FIG. 9. *Areal Growth of Oil Slick Based on Fay's (1969) Equations*

Scaling laws based on Froude, Reynolds, and Weber numbers would have to be invoked, along with a consideration of the relative values of the oil and water fluid properties—an impossible task. Obviously, the three initial mechanical spreading regimes are strongly affected by scale effects. For large volume prototype spills, the first two phases are significant, particularly gravity-viscous spreading. [Fay (1969) predicted that gravity-viscous spreading would dominate for a week, starting one hour after a 10,000 ton spill.] Small volume spills behave differently in that the surface tension phase is reached almost immediately. Spreading is also brought about by wave-induced turbulence and current shears, which are dependent on the Reynolds number and surf zone breaking wave characteristics. Although they have not formed part of this study, wind processes are of prime significance in field conditions, but would further complicate the model at small scale. It should also be noted that large-scale oil spills usually cover several surf zone widths when they reach the surf zone. In such cases, the nearshore circulation currents no longer act in an advective manner, but affect the oil spreading processes. Consequently, extrapolation of the above small-scale results to prototype scale is not possible. The U.S. Environmental Protection Agency gives a valuable account (*Proc.* 1989) of the scale-related problems faced when assessing oil bioremediation at the nearshore in the aftermath of the *Exxon Valdez* spillage.

Conclusions

This paper has considered the behavior of a small-scale (less than a surf zone width) oil slick in the nearshore zone. Reasonable agreement was

obtained between predicted and experimental nearshore circulation patterns for a specific beach topography. Discrepancies occurred due mainly to reflections from the smooth impermeable beach, which were not simulated in the numerical model. These may reduce for sandy or pebble beaches and where there are no lateral constraints. It is recommended that wave-current interaction models be based, in the first instance, on the mild slope equations, incorporating reflection, refraction, and diffraction.

Dyed cedar wood oil provided clear visualizations of the experimental slick. Using a digital image processor, the oil spread and thickness were determined. Allowing for differences in the wave-current field, the numerical model reasonably simulated the advection of the oil slick as it moved shorewards, alongshore, and then into the offshore rip current. The total oil spread (diffusion-type still water) coefficients, E_x and E_y, were obtained as 0.0004 m^2/s, substantially lower than determined by Murray (1972) and Hunter (1980) for the open sea, due to scale effects. Comparison with the experimental data indicated that the shape of the oil slick was well represented when it was transported by the on/offshore rip currents. Under the influence of the longshore current, both the numerical and experimental slicks became elliptical in shape, but stretched in different directions. In general, the numerical model underestimated the lateral spread of the oil, particularly when the slick came close to the stagnation zone at the center of the primary circulation cell. The major discrepancies were caused by underestimation of the wave heights (thus affecting the position of the breaker line) and the noninclusion of surface tension–viscous spreading in the numerical model.

Acknowledgments

The writers would like to express gratitude to Dr. K. Anastasiou of Imperial College, U.K. for his advice on certain computational aspects of this study. The second writer was originally funded by the Science and Engineering Research Council, SERC, U.K.

Appendix. References

Acops yearbook. (1991). Dept. of Energy, Acops, 3 Endsleigh St., London, U.K.

Battjes, J. A., and Janssen, J. P. F. M. (1978). "Energy loss and set-up due to breaking of random waves." *Proc., 16th Int. Conf. on Coastal Engrg.*, ASCE, New York, N.Y., 569–587.

Borthwick, A. G. L., and Joynes, S. A. (1989). "Nearshore circulation in the vicinity of a sinusoidal beach." *Hydrosoft J.*, 2(3), 106–118.

Copeland, G. J. M. (1985). "Practical radiation stress calculations connected with equations of wave propagation." *Coast. Engrg.*, 9(3), 195–219.

Crowley, W. P. (1968). "Numerical advection experiments." *Monthly Weather Rev.*, 1, 1–11.

Da Silva Lima, S. S. (1981). "Wave-induced nearshore circulation," PhD thesis, University of Liverpool, England.

DiPietro, N. D., Huh, C., and Cox, R. G. (1978). "The hydrodynamics of the spreading of one liquid on the surface of another." *J. Fluid Mech.*, 84(3), 529–549.

Elliott, A. J., Hurford, N., and Penn, C. J. (1986). "Shear diffusion and the spreading of oil slicks." *Mar. Pollut. Bull.*, 17(7), 308–313.

Fannelop, T. K., and Waldman, G. D. (1971). "The dynamics of oil slicks or creeping crude." *Paper No. 71-4*, American Institute of Aeronautics and Astronautics (AIAA), New York, N.Y.

Downloaded from ascelibrary.org by National Tech University Of Athens on 10/26/19. Copyright ASCE. For personal use only; all rights reserved.

Fay, J. A. (1969). "The spread of oil slicks on a calm sea." *Oil on the sea*, D. P. Hoult, ed., Plenum Press, New York, N.Y., 53–63.
Gundlach, E. R., Boehm, P. D., Marchand, M., Atlas, R. M., Ward, D. M., and Wolfe, D. A. (1983). "The fate of *Amoco Cadiz* oil." *Sci.*, 221(4606), 122–129.
Holly, F. M., and Usseglio-Polatera, J. M. (1984). "Dispersion simulation in two-dimensional tidal flow." *J. Hydr. Engrg.*, ASCE, 110(7), 905–925.
Huang, J. C. (1983). "A review of the state-of-the-art of oil spill/fate behavior models." *Proc., 1983 Oil Spill Conf.*, API, Washington, D.C., 313–322.
Hunter, J. R. (1980). "An interactive computer model of oil slick motion." *Proc., Oceanology Int. '80*, Brighton, U.K., 42–50.
"Impact of oil on the marine environment." (1977). *Report Study 6*, Food and Agriculture Organisation of the United Nations, Rome, Italy.
Johansen, O. (1985). *Particle-in-fluid model for simulation of oil drift and spread.* Oceanographic Centre, Sintef Group, Trondheim, Norway.
Joynes, S. A. (1989). "Horizontal diffusion of a buoyant pollutant in coastal waters," PhD thesis, University of Salford, England.
Kollmeyer, R. C., and Thompson, M. E. (1977). "New York Harbor oil drift prediction model." *Proc., 1977 Oil Spill Conf.*, API, Washington, D.C., 441–445.
Kolpack, R. L., Plutchak, N. B., and Stearns, R. W. (1977). "Fate of oil in a water environment. Phase II: A dynamic model of the mass balance for released oil." *Publication 4313*, API, Washington, D.C.
Kuipers, H. D. (1981). *A simulation model for oil slicks at sea.* Department of Civil Engineering, North Sea Directorate, Ministry of Transport and Public Works, Ijswijk, The Netherlands.
Kuiper, J., Wilde, P., and Wolff, W. (1984). "Effects of an oil spill in outdoor model tidal flat ecosystems." *Mar. Pollut. Bull.*, 15(3), 102–106.
Liu, P. L.-F., and Dalrymple, R. A. (1978). "Bottom frictional stresses and longshore currents due to waves with large angles of incidence." *J. Mar. Res.*, 36(2), 358–375.
Murray, S. P. (1972). "Turbulent diffusion of oil in the ocean." *J. Limnology and Oceanography*, 17(5), 651–659.
Noda, E. K. (1974). "Wave-induced nearshore circulation." *J. Geophys. Res.*, 79(27), 4097–4106.
Oil in the sea, inputs, fates, effects. (1985). National Research Council, National Academy Press, Washington, D.C.
Proc., of beach and nearshore workshop for Prince William Sound bioremediation project. (1989). S. C. McCutcheon, ed., U.S. Environmental Protection Agency, Athens, Ga.
Rasmussen, D. (1985). "Oil spill modelling—A tool for clean up operations." *Proc., 1985 Oil Spill Conf.*, API, Washington, D.C., 243–249.
Reed, M., and Gundlach, E. (1989). "Hindcast of the *Amoco Cadiz* event with a coastal zone oil spill model." *Oil Chem. Pollut.*, 5(6), 451–476.
Reed, M., Gundlach, E., and Kana, T. (1989). "A coastal zone oil spill model: Development and sensitivity studies." *Oil Chem. Pollut.*, 5(6), 411–449.
Shen, H. T., and Yapa, P. D. (1988). "Oil slick transport in rivers." *J. Hydr. Engrg.*, ASCE, 114(5), 529–543.
Shen, H. T., Yapa, P. D., and Petroski, M. E. (1987). "A simulation model for oil slick transport in lakes." *Water Resour. Res.*, 23(10), 1949–1957.
Spaulding, M. L. (1988). "A state-of-the-art review of oil spill trajectory and fate modelling." *Oil Chem. Pollut.*, 4, 39–55.
Stive, M. J. F., and Wind, H. G. (1986). "Cross-shore mean flow in the surf zone." *Coast. Engrg.*, 10(4), 325–340.
Swedmark, M., Granmo, A., and Kollberg, S. (1973). "Effects of oil dispersants and oil emulsions on marine animals." *Mar. Res.*, 7, 1649–1672.
Thornton, E. B. (1970). "Variation of longshore current across a surf zone." *Proc., 12th Int. Conf. Coastal Engrg.*, ASCE, New York, N.Y., 291–308.
Yapa, P. D., Thomas, R. J., Jr., Rutherford, R. S., and Shen, H. T. (1989). "Microcomputer model for oil spill simulation (MICROSS)." *J. Comput. Civ. Engrg.*, ASCE, 3(1), 33–46.

Downloaded from ascelibrary.org by National Tech University Of Athens on 10/26/19. Copyright ASCE. For personal use only; all rights reserved.